Measurement of the $\sigma(W+\geq 1\ \mathrm{Jet})/\sigma(W)$ Cross Section Ratio from $\bar{p}p$ Collisions at $\sqrt{s}=1.8$ TeV

F. Abe,[17] H. Akimoto,[39] A. Akopian,[31] M. G. Albrow,[7] A. Amadon,[5] S. R. Amendolia,[27] D. Amidei,[20] J. Antos,[33] S. Aota,[37] G. Apollinari,[31] T. Arisawa,[39] T. Asakawa,[37] W. Ashmanskas,[18] M. Atac,[7] P. Azzi-Bacchetta,[25] N. Bacchetta,[25] S. Bagdasarov,[31] M. W. Bailey,[22] P. de Barbaro,[30] A. Barbaro-Galtieri,[18] V. E. Barnes,[29] B. A. Barnett,[15] M. Barone,[9] G. Bauer,[19] T. Baumann,[11] F. Bedeschi,[27] S. Behrends,[3] S. Belforte,[27] G. Bellettini,[27] J. Bellinger,[40] D. Benjamin,[35] J. Bensinger,[3] A. Beretvas,[7] J. P. Berge,[7] J. Berryhill,[5] S. Bertolucci,[9] S. Bettelli,[27] B. Bevensee,[26] A. Bhatti,[31] K. Biery,[7] C. Bigongiari,[27] M. Binkley,[7] D. Bisello,[25] R. E. Blair,[1] C. Blocker,[3] S. Blusk,[30] A. Bodek,[30] W. Bokhari,[26] G. Bolla,[29] Y. Bonushkin,[4] D. Bortoletto,[29] J. Boudreau,[28] L. Breccia,[2] C. Bromberg,[21] N. Bruner,[22] R. Brunetti,[2] E. Buckley-Geer,[7] H. S. Budd,[30] K. Burkett,[20] G. Busetto,[25] A. Byon-Wagner,[7] K. L. Byrum,[1] M. Campbell,[20] A. Caner,[27] W. Carithers,[18] D. Carlsmith,[40] J. Cassada,[30] A. Castro,[25] D. Cauz,[36] A. Cerri,[27] P. S. Chang,[33] P. T. Chang,[33] H. Y. Chao,[33] J. Chapman,[20] M.-T. Cheng,[33] M. Chertok,[34] G. Chiarelli,[27] C. N. Chiou,[33] F. Chlebana,[7] L. Christofek,[13] M. L. Chu,[33] S. Cihangir,[7] A. G. Clark,[10] M. Cobal,[27] E. Cocca,[27] M. Contreras,[5] J. Conway,[32] J. Cooper,[7] M. Cordelli,[9] D. Costanzo,[27] C. Couyoumtzelis,[10] D. Cronin-Hennessy,[6] R. Culbertson,[5] D. Dagenhart,[38] T. Daniels,[19] F. DeJongh,[7] S. Dell'Agnello,[9] M. Dell'Orso,[27] R. Demina,[7] L. Demortier,[31] M. Deninno,[2] P. F. Derwent,[7] T. Devlin,[32] J. R. Dittmann,[6] S. Donati,[27] J. Done,[34] T. Dorigo,[25] N. Eddy,[20] K. Einsweiler,[18] J. E. Elias,[7] R. Ely,[18] E. Engels, Jr.,[28] W. Erdmann,[7] D. Errede,[13] S. Errede,[13] Q. Fan,[30] R. G. Feild,[41] Z. Feng,[15] C. Ferretti,[27] I. Fiori,[2] B. Flaugher,[7] G. W. Foster,[7] M. Franklin,[11] J. Freeman,[7] J. Friedman,[19] H. Frisch,[5] Y. Fukui,[17] S. Gadomski,[14] S. Galeotti,[27] M. Gallinaro,[26] O. Ganel,[35] M. Garcia-Sciveres,[18] A. F. Garfinkel,[29] C. Gay,[41] S. Geer,[7] D. W. Gerdes,[15] P. Giannetti,[27] N. Giokaris,[31] P. Giromini,[9] G. Giusti,[27] M. Gold,[22] A. Gordon,[11] A. T. Goshaw,[6] Y. Gotra,[28] K. Goulianos,[31] H. Grassmann,[36] L. Groer,[32] C. Grosso-Pilcher,[5] G. Guillian,[20] J. Guimaraes da Costa,[15] R. S. Guo,[33] C. Haber,[18] E. Hafen,[19] S. R. Hahn,[7] R. Hamilton,[11] T. Handa,[12] R. Handler,[40] F. Happacher,[9] K. Hara,[37] A. D. Hardman,[29] R. M. Harris,[7] F. Hartmann,[16] J. Hauser,[4] E. Hayashi,[37] J. Heinrich,[26] W. Hao,[35] B. Hinrichsen,[14] K. D. Hoffman,[29] M. Hohlmann,[5] C. Holck,[26] R. Hollebeek,[26] L. Holloway,[13] Z. Huang,[20] B. T. Huffman,[28] R. Hughes,[23] J. Huston,[21] J. Huth,[11] H. Ikeda,[37] M. Incagli,[27] J. Incandela,[7] G. Introzzi,[27] J. Iwai,[39] Y. Iwata,[12] E. James,[20] H. Jensen,[7] U. Joshi,[7] E. Kajfasz,[25] H. Kambara,[10] T. Kamon,[34] T. Kaneko,[37] K. Karr,[38] H. Kasha,[41] Y. Kato,[24] T. A. Keaffaber,[29] K. Kelley,[19] R. D. Kennedy,[7] R. Kephart,[7] D. Kestenbaum,[11] D. Khazins,[6] T. Kikuchi,[37] B. J. Kim,[27] H. S. Kim,[14] S. H. Kim,[37] Y. K. Kim,[18] L. Kirsch,[3] S. Klimenko,[8] D. Knoblauch,[16] P. Koehn,[23] A. Köngeter,[16] K. Kondo,[37] J. Konigsberg,[8] K. Kordas,[14] A. Korytov,[8] E. Kovacs,[1] W. Kowald,[6] J. Kroll,[26] M. Kruse,[30] S. E. Kuhlmann,[1] E. Kuns,[32] K. Kurino,[12] T. Kuwabara,[37] A. T. Laasanen,[29] S. Lami,[27] S. Lammel,[7] J. I. Lamoureux,[3] M. Lancaster,[18] M. Lanzoni,[27] G. Latino,[27] T. LeCompte,[1] S. Leone,[27] J. D. Lewis,[7] P. Limon,[7] M. Lindgren,[4] T. M. Liss,[13] J. B. Liu,[30] Y. C. Liu,[33] N. Lockyer,[26] O. Long,[26] C. Loomis,[32] M. Loreti,[25] D. Lucchesi,[27] P. Lukens,[7] S. Lusin,[40] J. Lys,[18] K. Maeshima,[7] P. Maksimovic,[11] M. Mangano,[27] M. Mariotti,[25] J. P. Marriner,[7] A. Martin,[41] J. A. J. Matthews,[22] P. Mazzanti,[2] P. McIntyre,[34] P. Melese,[31] M. Menguzzato,[25] A. Menzione,[27] E. Meschi,[27] S. Metzler,[26] C. Miao,[20] T. Miao,[7] G. Michail,[11] R. Miller,[21] H. Minato,[37] S. Miscetti,[9] M. Mishina,[17] S. Miyashita,[37] N. Moggi,[27] E. Moore,[22] Y. Morita,[17] A. Mukherjee,[7] T. Muller,[16] P. Murat,[27] S. Murgia,[21] M. Musy,[36] H. Nakada,[37] I. Nakano,[12] C. Nelson,[7] D. Neuberger,[16] C. Newman-Holmes,[7] C.-Y. P. Ngan,[19] L. Nodulman,[1] A. Nomerotski,[8] S. H. Oh,[6] T. Ohmoto,[12] T. Ohsugi,[12] R. Oishi,[37] M. Okabe,[37] T. Okusawa,[24] J. Olsen,[40] C. Pagliarone,[27] R. Paoletti,[27] V. Papadimitriou,[35] S. P. Pappas,[41] N. Parashar,[27] A. Parri,[9] J. Patrick,[7] G. Pauletta,[36] M. Paulini,[18] A. Perazzo,[27] L. Pescara,[25] M. D. Peters,[18] T. J. Phillips,[6] G. Piacentino,[27] M. Pillai,[30] K. T. Pitts,[7] R. Plunkett,[7] A. Pompos,[29] L. Pondrom,[40] J. Proudfoot,[1] F. Ptohos,[11] G. Punzi,[27] K. Ragan,[14] D. Reher,[18] M. Reischl,[16] A. Ribon,[25] F. Rimondi,[2] L. Ristori,[27] W. J. Robertson,[6] T. Rodrigo,[27] S. Rolli,[38] L. Rosenson,[19] R. Roser,[13] T. Saab,[14] W. K. Sakumoto,[30] D. Saltzberg,[4] A. Sansoni,[9] L. Santi,[36] H. Sato,[37] P. Schlabach,[7] E. E. Schmidt,[7] M. P. Schmidt,[41] A. Scott,[4] A. Scribano,[27] S. Segler,[7] S. Seidel,[22] Y. Seiya,[37] F. Semeria,[2] T. Shah,[19] M. D. Shapiro,[18] N. M. Shaw,[29] P. F. Shepard,[28] T. Shibayama,[37] M. Shimojima,[37] M. Shochet,[5] J. Siegrist,[18] A. Sill,[35] P. Sinervo,[14] P. Singh,[13] K. Sliwa,[38] C. Smith,[15] F. D. Snider,[15] J. Spalding,[7] T. Speer,[10] P. Sphicas,[19] F. Spinella,[27] M. Spiropulu,[11] L. Spiegel,[7] L. Stanco,[25] J. Steele,[40] A. Stefanini,[27] R. Ströhmer,[7,*] J. Strologas,[13] F. Strumia,[10] D. Stuart,[7] K. Sumorok,[19] J. Suzuki,[37] T. Suzuki,[37] T. Takahashi,[24] T. Takano,[24] R. Takashima,[12] K. Takikawa,[37] M. Tanaka,[37] B. Tannenbaum,[22] F. Tartarelli,[27] W. Taylor,[14] M. Tecchio,[20] P. K. Teng,[33] Y. Teramoto,[24] K. Terashi,[37] S. Tether,[19] D. Theriot,[7] T. L. Thomas,[22] R. Thurman-Keup,[1]

0031-9007/98/81(7)/1367(6)$15.00

M. Timko,[38] P. Tipton,[30] A. Titov,[31] S. Tkaczyk,[7] D. Toback,[5] K. Tollefson,[19] A. Tollestrup,[7] H. Toyoda,[24] W. Trischuk,[14] J. F. de Troconiz,[11] S. Truitt,[20] J. Tseng,[19] N. Turini,[27] T. Uchida,[37] F. Ukegawa,[26] J. Valls,[32] S. C. van den Brink,[28] S. Vejcik III,[20] G. Velev,[27] R. Vidal,[7] R. Vilar,[7,*] D. Vucinic,[19] R. G. Wagner,[1] R. L. Wagner,[7] J. Wahl,[5] N. B. Wallace,[27] A. M. Walsh,[32] C. Wang,[6] C. H. Wang,[33] M. J. Wang,[33] A. Warburton,[14] T. Watanabe,[37] T. Watts,[32] R. Webb,[34] C. Wei,[6] H. Wenzel,[16] W. C. Wester III,[7] A. B. Wicklund,[1] E. Wicklund,[7] R. Wilkinson,[26] H. H. Williams,[26] P. Wilson,[5] B. L. Winer,[23] D. Winn,[20] D. Wolinski,[20] J. Wolinski,[21] S. Worm,[22] X. Wu,[10] J. Wyss,[27] A. Yagil,[7] W. Yao,[18] K. Yasuoka,[37] G. P. Yeh,[7] P. Yeh,[33] J. Yoh,[7] C. Yosef,[21] T. Yoshida,[24] I. Yu,[7] A. Zanetti,[36] F. Zetti,[27] and S. Zucchelli[2]

(CDF Collaboration)

[1]*Argonne National Laboratory, Argonne, Illinois 60439*
[2]*Istituto Nazionale di Fisica Nucleare, University of Bologna, I-40127 Bologna, Italy*
[3]*Brandeis University, Waltham, Massachusetts 02254*
[4]*University of California at Los Angeles, Los Angeles, California 90024*
[5]*University of Chicago, Chicago, Illinois 60637*
[6]*Duke University, Durham, North Carolina 27708*
[7]*Fermi National Accelerator Laboratory, Batavia, Illinois 60510*
[8]*University of Florida, Gainesville, Florida 32611*
[9]*Laboratori Nazionali di Frascati, Istituto Nazionale di Fisica Nucleare, I-00044 Frascati, Italy*
[10]*University of Geneva, CH-1211 Geneva 4, Switzerland*
[11]*Harvard University, Cambridge, Massachusetts 02138*
[12]*Hiroshima University, Higashi-Hiroshima 724, Japan*
[13]*University of Illinois, Urbana, Illinois 61801*
[14]*Institute of Particle Physics, McGill University, Montreal, Canada H3A 2T8 and University of Toronto, Toronto, Canada M5S 1A7*
[15]*The Johns Hopkins University, Baltimore, Maryland 21218*
[16]*Institut für Experimentelle Kernphysik, Universität Karlsruhe, 76128 Karlsruhe, Germany*
[17]*National Laboratory for High Energy Physics (KEK), Tsukuba, Ibaraki 305, Japan*
[18]*Ernest Orlando Lawrence Berkeley National Laboratory, Berkeley, California 94720*
[19]*Massachusetts Institute of Technology, Cambridge, Massachusetts 02139*
[20]*University of Michigan, Ann Arbor, Michigan 48109*
[21]*Michigan State University, East Lansing, Michigan 48824*
[22]*University of New Mexico, Albuquerque, New Mexico 87131*
[23]*The Ohio State University, Columbus, Ohio 43210*
[24]*Osaka City University, Osaka 588, Japan*
[25]*Università di Padova, Istituto Nazionale di Fisica Nucleare, Sezione di Padova, I-35131 Padova, Italy*
[26]*University of Pennsylvania, Philadelphia, Pennsylvania 19104*
[27]*Istituto Nazionale di Fisica Nucleare, University and Scuola Normale Superiore of Pisa, I-56100 Pisa, Italy*
[28]*University of Pittsburgh, Pittsburgh, Pennsylvania 15260*
[29]*Purdue University, West Lafayette, Indiana 47907*
[30]*University of Rochester, Rochester, New York 14627*
[31]*Rockefeller University, New York, New York 10021*
[32]*Rutgers University, Piscataway, New Jersey 08855*
[33]*Academia Sinica, Taipei, Taiwan 11530, Republic of China*
[34]*Texas A&M University, College Station, Texas 77843*
[35]*Texas Tech University, Lubbock, Texas 79409*
[36]*Istituto Nazionale di Fisica Nucleare, University of Trieste/Udine, Italy*
[37]*University of Tsukuba, Tsukuba, Ibaraki 315, Japan*
[38]*Tufts University, Medford, Massachusetts 02155*
[39]*Waseda University, Tokyo 169, Japan*
[40]*University of Wisconsin, Madison, Wisconsin 53706*
[41]*Yale University, New Haven, Connecticut 06520*

(Received 28 April 1998)

The ratio of the $W+\geq 1$ jet cross section to the inclusive W cross section is measured using $W^{\pm}\rightarrow e^{\pm}\nu$ events from $\overline{p}p$ collisions at $\sqrt{s}=1.8$ TeV. The data are from 108 pb^{-1} of integrated luminosity collected with the Collider Detector at Fermilab. Measurements of the cross section ratio for jet transverse energy thresholds ($E_T^{\min}$) ranging from 15 to 95 GeV are compared to theoretical predictions using next-to-leading-order QCD calculations. Data and theory agree well for $E_T^{\min}>25$ GeV, where the predictions lie within 1 standard deviation of the measured values. [S0031-9007(98)06871-9]

PACS numbers: 13.87.Ce, 12.38.Qk, 13.85.Qk

The measurement of jet properties in W boson events from $\overline{p}p$ collisions can be used to test perturbative quantum chromodynamics (QCD) at large momentum transfers. In previous studies by the CDF Collaboration, jet production properties in W and Z boson events were compared to leading-order (LO) QCD predictions [1,2]. In this Letter, we test QCD predictions at next-to-leading order (NLO) by measuring the cross section ratio $\mathcal{R}_{10} = \sigma(W+ \geq 1 \text{ jet})/\sigma(W)$. Measurements of W + jet cross section ratios by the UA2 and UA1 Collaborations agreed well with theoretical predictions and allowed measurements of the strong coupling constant α_s [3,4]. Recent measurements from the D0 Collaboration, however, indicate a discrepancy between ratios of W + jet cross sections and NLO QCD predictions [5,6].

We measure $\mathcal{R}_{10}$ using 51 437 $W^{\pm} \rightarrow e^{\pm}\nu$ candidates observed at the Collider Detector at Fermilab (CDF) [7]. The principal detector elements used for this analysis are the central tracking chamber (CTC), vertex tracking chamber (VTX), and the calorimeters. The CTC is a cylindrical drift chamber that measures the momenta of charged particles in the pseudorapidity range $|\eta| < 1.1$ [8]. The VTX, a time-projection chamber, identifies interactions along the beam direction. Both tracking detectors are immersed in a 1.4 T solenoidal magnetic field. The electromagnetic and hadronic calorimeters, segmented in a projective tower geometry, cover the range $|\eta| < 4.2$ and measure the energies of electrons, photons, and jets.

The $W \rightarrow e\nu$ candidates are selected from events that pass a high transverse energy ($E_T = E \sin\theta$) electron trigger. The event selection requires an isolated electron [9] in the fiducial region of the central calorimeter ($|\eta| \leq 1.1$). The electron must have $E_T \geq 20$ GeV and satisfy tight selection criteria [10]. The reconstructed transverse energy of the neutrino, measured from the imbalance of E_T in the calorimeter ($\not{E}_T$) [11], must exceed 30 GeV. Jets in the W events are reconstructed by clustering energy depositions in the calorimeter using a cone algorithm [12] with radius $\Delta R \equiv \sqrt{(\Delta\eta)^2 + (\Delta\phi)^2} = 0.4$. This cone size was used for previous W and Z + jet analyses [1,2]. The jet E_T is corrected for calorimeter response, underlying event energy within the jet cone, and energy contamination from additional $\overline{p}p$ interactions in the same bunch crossing [13]. Jets with $|\eta| \leq 2.4$ are selected for this analysis. To ensure that jets are well separated from electrons, an event is rejected if any jet with $E_T \geq 12$ GeV lies within $\Delta R = 0.52$ of an electron.

We obtain $\mathcal{R}_{10}$ by dividing the $W+ \geq 1$ jet cross section for a particular minimum jet E_T threshold (E_T^{min}) by the inclusive W cross section. The cross section ratio measurement is corrected for backgrounds, acceptances, and efficiencies. Measuring a ratio of cross sections takes advantage of the cancellation of the integrated luminosity, and many systematic uncertainties are reduced. In this analysis, we measure $\mathcal{R}_{10}$ for values of E_T^{min} that range from 15 to 95 GeV in 5 GeV increments. Of 51 437 $W \rightarrow e\nu$ candidates, 7905 events have ≥ 1 with $E_T > 15$ GeV, and 214 events have ≥ 1 jet with $E_T > 95$ GeV.

TABLE I. Backgrounds (%) in the $W+ \geq 1$ jet sample.

	E_T^{min} (GeV) 15	55	95
QCD multijet	13 ± 4	14 ± 5	28 ± 13
$W \rightarrow \tau\nu$	2.9 ± 0.3	7.8 ± 1.2	6.4 ± 2.4
$Z \rightarrow e^+e^-$	1.8 ± 0.1	2.3 ± 0.2	2.2 ± 0.4
$Z \rightarrow \tau^+\tau^-$	0.6 ± 0.1	1.8 ± 0.1	1.8 ± 0.3
Top	0.5 ± 0.1	3.1 ± 0.6	5.1 ± 1.0
X jet, $W\gamma$	3.6 ± 3.6	0.3 ± 0.3	0.3 ± 0.3

The sources of background in the $W+ \geq 1$ jet sample are summarized in Table I for $E_T^{\text{min}} = 15$, 55, and 95 GeV. The largest background to $W \rightarrow e\nu$ production arises from QCD multijet production. In some multijet events, a jet is incorrectly reconstructed as an electron and a large $\not{E}_T$ results from shower fluctuations or uninstrumented regions in the calorimeter. We measure this multijet contamination using an event sample obtained by removing the electron isolation and $\not{E}_T$ requirements of the W selection [11]. The backgrounds also include several electroweak processes that yield an electron and $\not{E}_T$ in the final state. We calculate backgrounds from $W \rightarrow \tau\nu$ (with $\tau \rightarrow e\nu\overline{\nu}$), $Z \rightarrow \tau^+\tau^-$, and $Z \rightarrow e^+e^-$ (where one electron is not identified) using the VECBOS Monte Carlo program [14] and a simulation of the CDF detector. The background calculation also removes a contribution from standard model $t\overline{t}$ production, in which one of the top quarks decays via $t \rightarrow Wb \rightarrow e\nu b$. In addition to these backgrounds, the number of ≥ 1 jet events is corrected to account for jets produced by additional $\overline{p}p$ interactions ("X jets") and $W\gamma$ events in which the photon is reconstructed as a jet. The total $W+ \geq 1$ jet background increases from (22 ± 5)% at $E_T^{\text{min}} = 15$ GeV to (44 ± 13)% at $E_T^{\text{min}} = 95$ GeV. The overall background to inclusive W events is (5.9 ± 1.2)%.

The acceptance for $W \rightarrow e\nu$ events, which corrects for losses due to the fiducial and kinematic requirements on the electron and $\not{E}_T$, is determined for each E_T^{min} using VECBOS [14] and a CDF detector simulation. As shown in Table II, the acceptance for $W+ \geq 1$ jet events increases with E_T^{min} from 24% to 36%. The acceptance for inclusive W events is (23.9 ± 0.5)%.

Table II also lists the efficiencies for detecting $W \rightarrow e\nu$ events, which include the trigger efficiency, the electron identification (ID) efficiency, and the electron-jet

TABLE II. $W^{\pm} \rightarrow e^{\pm}\nu$ acceptance and efficiencies (in %) for the $W+ \geq 1$ jet sample.

	E_T^{min} (GeV) 15	55	95
Acceptance	24 ± 1	29 ± 1	36 ± 2
Trigger	95 ± 1	94 ± 2	93 ± 2
Electron ID	88 ± 1	84 ± 5	77 ± 13
Electron-jet overlap	94 ± 1	95 ± 1	96 ± 3

TABLE III. Measured values of $\mathcal{R}_{10} = \sigma(W+ \geq 1 \text{ jet})/\sigma(W)$ for $E_T^{\min}$ ranging from 15 to 95 GeV, compared to QCD predictions using MRSA$'$ with $Q_r = Q_f = M_W$. The uncertainties on $\mathcal{R}_{10}$(data) are statistical and systematic, respectively.

$E_T^{\min}$ (GeV)	$\mathcal{R}_{10}$(data)	$\mathcal{R}_{10}$(QCD)
15	0.1301 ± 0.0057 ± 0.0102	0.1557
20	0.0868 ± 0.0043 ± 0.0070	0.1036
25	0.0649 ± 0.0035 ± 0.0053	0.0718
30	0.0484 ± 0.0028 ± 0.0039	0.0515
35	0.0363 ± 0.0023 ± 0.0029	0.0377
40	0.0275 ± 0.0019 ± 0.0025	0.0284
45	0.0215 ± 0.0017 ± 0.0019	0.0217
50	0.0161 ± 0.0014 ± 0.0015	0.0166
55	0.0126 ± 0.0012 ± 0.0012	0.0129
60	0.0097 ± 0.0011 ± 0.0011	0.0102
65	0.0072 ± 0.0009 ± 0.0009	0.0080
70	0.0054 ± 0.0007 ± 0.0007	0.0063
75	0.0044 ± 0.0007 ± 0.0006	0.0051
80	0.0037 ± 0.0006 ± 0.0006	0.0041
85	0.0028 ± 0.0006 ± 0.0004	0.0033
90	0.0025 ± 0.0006 ± 0.0004	0.0027
95	0.0019 ± 0.0005 ± 0.0004	0.0022

overlap efficiency. The electron-jet overlap efficiency accounts for losses from the electron-jet separation requirement and from jets that overlap electrons in the calorimeter. The electron ID and electron-jet overlap efficiencies are measured from the data using $Z \rightarrow e^+e^-$ events. The combined $W \rightarrow e\nu$ acceptance and detection efficiency is (19.5 ± 0.5)% for the inclusive W sample. For the $W+ \geq 1$ jet sample, it ranges from (19 ± 1)% at $E_T^{\min} = 15$ GeV to (25 ± 3)% at $E_T^{\min} = 95$ GeV.

One of the large systematic uncertainties on $\mathcal{R}_{10}$ is the jet energy scale uncertainty, which includes calorimeter response and the amount of underlying event energy deposited in the jet cone. Varying the jet energy scale by 1 standard deviation yields a systematic uncertainty on $\mathcal{R}_{10}$ that ranges from 5% at $E_T^{\min} = 15$ GeV to 11% at $E_T^{\min} = 95$ GeV. Uncertainties in the QCD multijet background result in a 4% to 14% systematic uncertainty on $\mathcal{R}_{10}$. Other sources of systematic uncertainty on $\mathcal{R}_{10}$ include the $W \rightarrow e\nu$ acceptance, electron-jet overlap efficiency, top quark background, and jet backgrounds from additional interactions and $W\gamma$ production. The overall systematic uncertainty on $\mathcal{R}_{10}$ ranges from 8% at $E_T^{\min} = 15$ GeV to 19% at $E_T^{\min} = 95$ GeV.

The measured values of $\mathcal{R}_{10}$ for $E_T^{\min} = 15$ to 95 GeV are listed in Table III. We compare these measurements to perturbative QCD predictions generated using the DYRAD [15] Monte Carlo program. DYRAD calculates NLO matrix elements for W inclusive (order α_s) and $W+ \geq 1$ jet (order α_s^2) production. The cross sections are computed by DYRAD for a particular renormalization scale Q_r and a set of parton distribution functions (PDF) with parton momentum fractions calculated at a factorization scale Q_f. Using the value of Λ_{QCD} associated with the PDF, the strong coupling constant α_s is evolved to

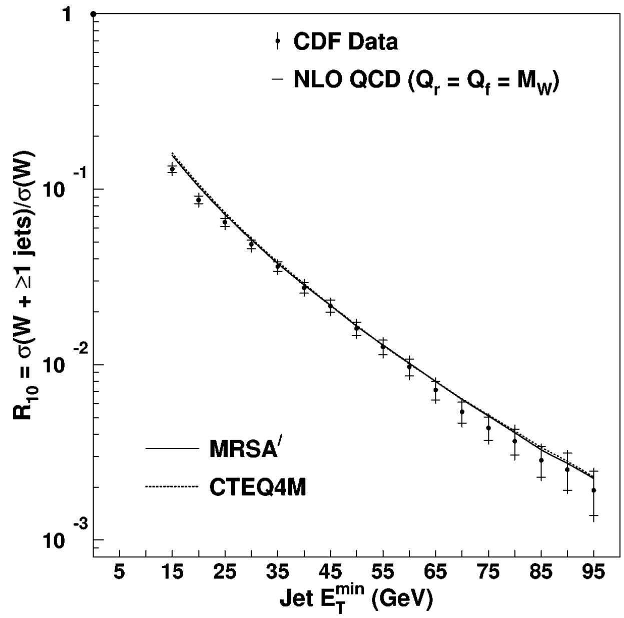

FIG. 1. $\mathcal{R}_{10}$ measurement vs jet $E_T^{\min}$, compared to NLO QCD predictions calculated using the MRSA$'$ and CTEQ4M parton distribution functions. The renormalization and factorization scales are set equal to the W boson mass. The inner error bars include statistical uncertainties only; the outer error bars include both statistical and systematic uncertainties. Note that the measurements of $\mathcal{R}_{10}$ at each value of $E_T^{\min}$ are statistically correlated because the corresponding event samples are not independent.

the scale Q_r using the second-order expression for the running coupling constant (two-loop α_s).

The theoretical predictions for $\mathcal{R}_{10}$ are found by dividing the DYRAD $W+ \geq 1$ jet cross section by the inclusive W cross section for a particular PDF, Q_r, and Q_f. At NLO, the $W+ \geq 1$ jet cross section calculation includes diagrams with up to two partons (order α_s^2) in the final state. When two partons have $\Delta R < 0.52$, their 4-vectors are added vectorially to form a jet. This parton clustering simulates the 0.4 cone algorithm used to reconstruct jets in the calorimeter, which can resolve pairs

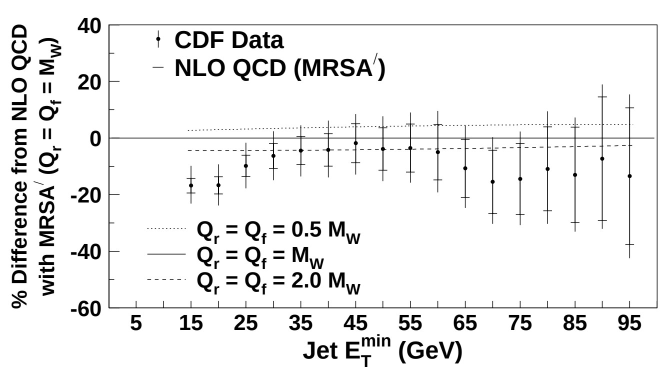

FIG. 2. Ratio of $\mathcal{R}_{10}$(data) − $\mathcal{R}_{10}$(QCD) to $\mathcal{R}_{10}$(QCD) for MRSA$'$ using $Q_r = Q_f = M_W$ (points). The superimposed curves show the sensitivity of the NLO QCD prediction to the renormalization and factorization scales, which are set to 0.5 and 2.0 times the W boson mass.

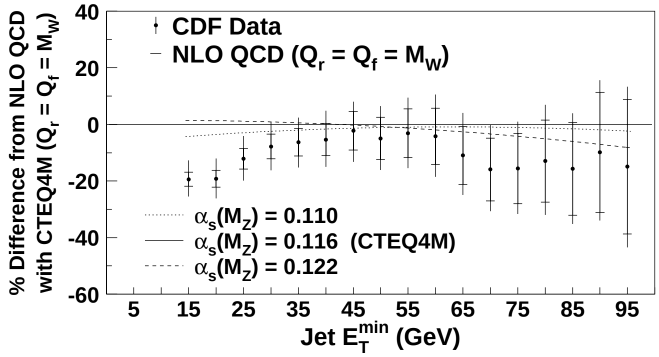

FIG. 3. Ratio of $\mathcal{R}_{10}$(data) − $\mathcal{R}_{10}$(QCD) to $\mathcal{R}_{10}$(QCD) for CTEQ4M using $Q_r = Q_f = M_W$ (points). Curves are superimposed for other PDFs in the CTEQ4 family with $\alpha_s(M_Z)$ values ranging from 0.110 to 0.122.

of jets that are separated in ΔR by at least 1.3 times the jet cone size [12]. After jets are smeared in E_T, η, and ϕ to model detector resolution effects [16,17], events that have one or more jets with $E_T > E_T^{\min}$ and $|\eta| < 2.4$ are used to calculate the final $W+ \geq 1$ jet cross section.

Because jet energies are measured in the data without corrections for energy deposited outside of the jet cone, the measurement of $\mathcal{R}_{10}$ depends on jet cone size. The NLO $W+ \geq 1$ jet calculations approximate the shape of jets by producing up to two final-state partons. Therefore, the agreement between data and theory depends on how accurately the theory reproduces the shape of jets.

The measured and predicted values of $\mathcal{R}_{10}$ are compared as a function of $E_T^{\min}$ in Fig. 1. The NLO QCD predictions for two different PDF sets, MRSA′ [18] and CTEQ4M [19], are represented by smooth curves that pass through the calculated values of $\mathcal{R}_{10}$ at each $E_T^{\min}$. The renormalization and factorization scales are set equal to the W boson mass. Data and theory agree well for $E_T^{\min} > 25$ GeV. At $E_T^{\min} = 0$, the measured value of $\mathcal{R}_{10}$ is unity by definition, whereas the NLO QCD prediction diverges. In addition, soft gluon effects that are not included in the DYRAD calculation may be significant in the low $E_T^{\min}$ region. The effect of changing the parton clustering algorithm is small. Varying the ΔR requirement of 0.52 by ±30% yields a change in $\mathcal{R}_{10}$ of less than 10% for all $E_T^{\min}$.

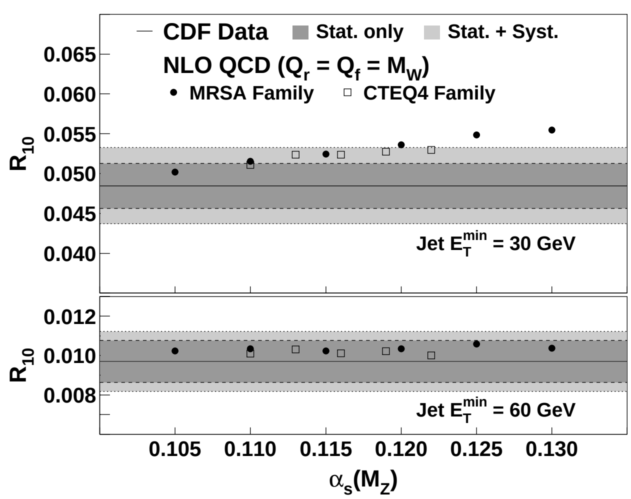

FIG. 4. $\mathcal{R}_{10}$ vs $\alpha_s(M_Z)$ for PDFs in the MRSA and CTEQ4 families. The symbols represent the predicted values of $\mathcal{R}_{10}$ at $E_T^{\min} = 30$ GeV (top) and $E_T^{\min} = 60$ GeV (bottom), compared to the measured values (shaded bands).

Figure 2 shows a plot of $[\mathcal{R}_{10}(\text{data}) - \mathcal{R}_{10}(\text{QCD})]/\mathcal{R}_{10}(\text{QCD})$ using MRSA′ with $Q_r = Q_f = M_W$. Curves are superimposed for predictions evaluated at two other scales: $Q_r = Q_f = 0.5M_W$ and $Q_r = Q_f = 2.0M_W$. Compared to LO QCD predictions (also generated using DYRAD), the NLO QCD predictions are significantly less sensitive to scale variations; varying Q_r and Q_f together by a factor of 2 results in a 5% change in $\mathcal{R}_{10}$ at NLO compared to a 15% change at LO. For $Q_r = Q_f = M_W$, the LO and NLO QCD predictions differ by less than 10% over the entire range of $E_T^{\min}$.

A plot of $[\mathcal{R}_{10}(\text{data}) - \mathcal{R}_{10}(\text{QCD})]/\mathcal{R}_{10}(\text{QCD})$ using CTEQ4M with $Q_r = Q_f = M_W$ is shown in Fig. 3. Curves are superimposed for other PDFs in the CTEQ4 family, fit with $\alpha_s(M_Z)$ values ranging from 0.110 to 0.122. The predictions for $\mathcal{R}_{10}$ show very little sensitivity to variations in α_s. Figure 4 shows a plot of $\mathcal{R}_{10}$ vs $\alpha_s(M_Z)$ for several PDF sets in the MRSA [20] and CTEQ4 families. The measured values of $\mathcal{R}_{10}$, given for $E_T^{\min} = 30$ GeV and $E_T^{\min} = 60$ GeV, are represented by horizontal bands. The data and theory are consistent for values of α_s ranging from 0.105 to 0.130.

In summary, we have measured the cross section ratio $\mathcal{R}_{10} = \sigma(W+ \geq 1\ \text{jet})/\sigma(W)$ in $W^\pm \rightarrow e^\pm \nu$ events from 108 pb^{-1} of $\bar{p}p$ collisions at $\sqrt{s} = 1.8$ TeV. The cross section ratio is fully corrected for $W \rightarrow e\nu$ backgrounds, acceptances, and efficiencies. Using jets with a cone size of 0.4 in the region $|\eta| < 2.4$, we observe good agreement between data and theory for $E_T^{\min} > 25$ GeV, where the predictions lie within 1 standard deviation of the measured values. The small dependence of $\mathcal{R}_{10}$ to variations in α_s, however, precludes an extraction of α_s from this measurement.

We thank the Fermilab staff and the technical staffs of the participating institutions for their vital contributions. We also thank Walter Giele and Nigel Glover for many useful discussions. This work was supported by the U.S. Department of Energy and National Science Foundation, the Italian Istituto Nazionale di Fisica Nucleare, the Ministry of Education, Science and Culture of Japan, the Natural Sciences and Engineering Research Council of Canada, the National Science Council of the Republic of China, the A. P. Sloan Foundation, and the Swiss National Science Foundation.

*Visitor.

[1] F. Abe *et al.*, Phys. Rev. Lett. **79**, 4760 (1997).
[2] F. Abe *et al.*, Phys. Rev. Lett. **77**, 448 (1996).
[3] J. Alitti *et al.*, Phys. Lett. B **263**, 563 (1991).

[4] M. Lindgren *et al.*, Phys. Rev. D **45**, 3038 (1992).
[5] S. Abachi *et al.*, Phys. Rev. Lett. **75**, 3226 (1995).
[6] B. Abbott *et al.*, Fermilab Report No. FERMILAB-CONF-97-369-E.
[7] F. Abe *et al.*, Nucl. Instrum. Methods Phys. Res., Sect. A **271**, 387 (1988).
[8] We use a coordinate system in which z is along the proton direction, ϕ is the azimuthal angle, θ is the polar angle, and $\eta \equiv -\ln(\tan\frac{\theta}{2})$ is the pseudorapidity. We take $z = 0$ at the center of the detector for fiducial cuts and at the interaction point for event variables.
[9] An isolated electron is one for which the calorimeter E_T in a cone of radius 0.4 in η-ϕ around the electron cluster in less than 10% of the electron E_T.
[10] F. Abe *et al.*, Phys. Rev. D **44**, 29 (1991); our selection is the same as in this reference except for (i) $0.5 < E/pc < 2.0$ and (ii) $\chi^2_{\text{strip}} < 10$.
[11] F. Abe *et al.*, Phys. Rev. D **52**, 2624 (1995).
[12] F. Abe *et al.*, Phys. Rev. D **45**, 1448 (1992).
[13] F. Abe *et al.*, Phys. Rev. D **47**, 4857 (1993).
[14] F. A. Berends, W. T. Giele, H. Kuijf, and B. Tausk, Nucl. Phys. **B357**, 32 (1991).
[15] W. T. Giele, E. W. N. Glover, and D. A. Kosower, Nucl. Phys. **B403**, 633 (1993).
[16] F. Abe *et al.*, Phys. Rev. D **57**, 67 (1998), with minor modifications for 0.4 jet cones.
[17] J. R. Dittmann, Ph.D. thesis, Duke University, 1998.
[18] A. D. Martin, R. G. Roberts, and W. J. Stirling, Phys. Lett. B **354**, 155 (1995).
[19] H. L. Lai *et al.*, Phys. Rev. D **55**, 1280 (1997).
[20] A. D. Martin, R. G. Roberts, and W. J. Stirling, Phys. Lett. B **356**, 89 (1995).